**Atmospheric
Chemistry
and Physics
Discussions**

Physical properties of iodate solutions and the deliquescence of crystalline I_2O_5 and HIO_3

R. Kumar[1], R. W. Saunders[1], A. S. Mahajan[1,*], J. M. C. Plane[1], and B. J. Murray[1]

[1]School of Chemistry, University of Leeds, Leeds LS2 9JT, UK
[*]current address: Laboratory for Atmospheric and Climate Science (CIAC), CSIC, 45007 Toledo, Spain

Abstract

Secondary aerosol produced from marine biogenic sources in algal-rich coastal locations will initially be composed of iodine oxide species, most likely I_2O_5, or its hydrated form HIO_3, formed as a result of iodine gas-phase chemistry. At present, there is no
5 quantitative hygroscopic data for these compounds and very little data available for iodate solutions (HIO_3 and I_2O_5 share a common aqueous phase). With increased interest in the role of such aerosol in the marine atmosphere, we have conducted studies of (i) the deliquescence behaviour of crystalline HIO_3 and I_2O_5 at 273–303 K, (ii) the efflorescence behaviour of aqueous iodate solution droplets, and (iii) properties (water
10 activity, density, and viscosity) of subsaturated and saturated iodate solutions.
   The deliquescence of I_2O_5 crystals at 293 K was observed to occur at a relative humidity (DRH) of $80.8 \pm 1.0\%$, whereas for HIO_3, a DRH of $85.0 \pm 1.0\%$ was measured. These values are consistent with measured water activity values for saturated I_2O_5 and HIO_3 solutions at 293 K of 0.80 ± 0.01 and 0.84 ± 0.01 respectively. At all temperatures,
15 DRH values for HIO_3 crystals were observed to be higher than for those of I_2O_5. The temperature-dependent DRH data, along with solubility and water activity data were used to evaluate the enthalpy of solution (ΔH_{sol}) for HIO_3 and I_2O_5. A ΔH_{sol} value of $8.3 \pm 0.7 \, \text{kJ mol}^{-1}$ was determined for HIO_3 which is consistent with a literature value of $8.8 \, \text{kJ mol}^{-1}$. For I_2O_5, we report for the first time its solubility at various temperatures
20 and $\Delta H_{sol} = 12.4 \pm 0.6 \, \text{kJ mol}^{-1}$. The measured water activity values confirm that aqueous iodate solutions are strongly non-ideal, consistent with previous reports of complex ion formation and molecular aggregation.

1   Introduction

Aerosols play an important role in many processes affecting the atmospheric chemistry
25 and climate of the Earth (Seinfeld and Pandis, 2006). They can alter the Earth's radiative balance either directly by the scattering of solar radiation, or indirectly by acting as

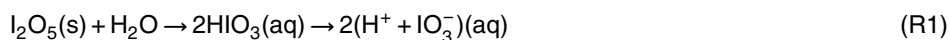cloud condensation nuclei (CCN) and ice nuclei (IN) (McFiggans et al., 2006).

For a thorough knowledge of the physical behaviour of aerosol in the atmosphere, a comprehensive understanding of critical properties (e.g. water activity – a_w, density – ρ, and viscosity – η) of aqueous solutions, and deliquescence data of relevant compounds is necessary. For some inorganic compounds (primarily sodium and ammonium salts), such data has been extensively reported in the literature (Martin, 2000) and has been used in chemical-thermodynamic modelling of single component and mixed aerosol systems (Clegg et al., 1998; Wexler and Clegg, 2002; Topping et al., 2005).

The transformation from a solid crystalline phase to an aqueous solution usually occurs at a narrowly defined threshold value, known as the deliquescence relative humidity (DRH). Conversely, when RH decreases, an aqueous solution droplet first shrinks because of water evaporation and finally crystallises at a lower threshold RH (below the DRH), known as the efflorescence relative humidity (ERH) (Seinfeld and Pandis, 2006).While deliquescence is a thermodynamically controlled transition, efflorescence is kinetically controlled.

A direct link between biogenic iodine vapour release at coastal sites and aerosol formation has been firmly established through field campaigns (O'Dowd et al., 2002a; McFiggans et al., 2010) with supporting laboratory studies (e.g. O'Dowd et al., 2002b; McFiggans et al., 2004; Burkholder et al., 2004; Saunders and Plane, 2005). Whilst the speciation of iodine, primarily the ionic forms, iodate (IO_3^-) and iodide (I^-), within marine aerosol has been discussed (Pechtl et al., 2007; Gilfedder et al., 2008), the relatively recent cited studies of coastal secondary particle formation involving iodine oxides (see O'Dowd and De Leeuw, 2007 and references therein), with the possibility of such aerosol also being important in open-ocean and polar environments (Mahajan et al., 2010; Saiz-Lopez et al., 2007), has necessitated a greater understanding of the solid-phase species I_2O_4, I_2O_5 and HIO_3, as well as their aqueous phases. In this study we focus on I_2O_5 and HIO_3 since I_2O_4 slowly disproportionates to I_2(aq/s) and HIO_3(aq) in water (Daehlie and Kjekshus, 1964). Dissolution of both of these crystalline

solids (I_2O_5 and HIO_3) leads to a common iodate (IO_3^-) aqueous phase;

$$I_2O_5(s) + H_2O \rightarrow 2HIO_3(aq) \rightarrow 2(H^+ + IO_3^-)(aq) \tag{R1}$$

$$HIO_3(s) + H_2O \rightarrow H^+(aq) + IO_3^-(aq) \tag{R2}$$

Hence, while it is expected that the crystals will have different physical properties, their aqueous solutions will be identical. In this paper we express the concentration of solutions made with both solids as the formal molality of iodate [$m(IO_3^-)$]. For HIO_3, $m(IO_3^-)$ is simply $m(HIO_3)$ while for I_2O_5 we can state:

$$m\left(IO_3^-\right) = m(I_2O_5) \times \left[\frac{\text{moles of } H_2O}{\text{moles of } H_2O - \text{moles of } I_2O_5} \right] \times 2 \tag{1}$$

where $m(I_2O_5)$ is the solution molality of I_2O_5.

Appropriate physical data for I_2O_5 and HIO_3 is sparse in the literature. Some iodate solution properties are reported in studies which date back over more than a century (Groschuff, 1905; Nayar et al., 1939; Goldman et al., 1974; Strong and Pethybridge, 1987), but there is a lack of sufficiently detailed data available and therefore an assessment of the potential climatic impact of these aerosol-forming compounds is currently not possible.

In this study, our motivation was to provide the underpinning physical knowledge required to improve the understanding of solid and aqueous phase iodine oxide particles (IOPs). This study is focused on the deliquescence behaviour of I_2O_5 and HIO_3 crystals in addition to various physical properties (water activity, density and viscosity) of aqueous iodate solutions. We also report our attempt to study the efflorescence of iodate solutions at low relative humidity.

2 Experimental

2.1 Water activity measurements

A number of iodate solutions were prepared from crystalline I_2O_5 and HIO_3 (I_2O_5: 99.99%, Sigma-Aldrich and HIO_3: ≥99.5%, Sigma-Aldrich) in 18.2 MΩ ultra-pure water, spanning a molality (m) range up to and including that of a saturated solution of HIO_3 (m=17.3 moles kg^{-1}/75.3 wt%) and of I_2O_5 (m=7.8 moles kg^{-1}/72.2 wt%) at 293 K.

Water activities [$a_w(T) = p(T)/p^o(T)$; where $p(T)$ is the equilibrium vapour pressure above a solution surface at temperature T and $p^o(T)$ is the vapour pressure above pure water at the same temperature] of aqueous solutions were measured directly using an automated activity meter (Aqualab series 3TE, Decagon Devices Inc.; accuracy ± 0.003). The instrument utilizes the chilled mirror dew-point technique to determine the dew point of air in equilibrium with a solution. The instrument was calibrated before each I_2O_5 and HIO_3 solution measurement using both pure water (a_w=1) and an aqueous solution of LiCl (13.41 m, a_w=0.25) (Stoloff, 1978).

2.2 Density measurements

The densities of a series of I_2O_5 and HIO_3 solutions were measured at 293 K. All solutions were carefully prepared in volumetric flasks by dissolving the respective solids in 18.2 MΩ ultra pure water and densities were determined by gravimetric analysis using a precision weighing balance (accuracy of 0.1 mg).

2.3 Viscosity measurements

The viscosities of the high molality ($17.6 < m(IO_3^-) < 15.8$ moles kg^{-1}) solutions were measured over the temperature range of 293–303 K using a falling ball viscometer (Gilmont GV-2300, size-3). Approximately 7 ml of each solution were placed into the tube of the viscometer which was immersed in a large beaker of water, placed onto

a heating/magnetic stirring plate. The water was heated to the desired temperature (measured with a K-type thermocouple) and stirred continuously. The viscometer was then left for ~30 min to equilibrate with the water temperature. The descent times of the ball in each solution were then measured a number of times (typically 10 for each solution and temperature) and the average time was used to determine the dynamic viscosity (η/cP) of the solution from the formula:

$$\eta = K(\rho_t - \rho)t \tag{2}$$

Where, ρ_t is the density of the ball (g cm^{-3}), ρ is the density of liquid (g cm^{-3}), t is the time of descent (minutes) and K is the viscometer constant (for the size-3 viscometer, the value of K is 35).

A 99% glycerol solution (Aldrich) was used initially to verify the performance of the viscometer. Measured solution viscosities at a number of temperatures were found to agree to within 5% of those reported in the literature (Segur and Oberstar, 1951).

2.4 Deliquescence and efflorescence measurements

Deliquescence and efflorescence behaviour of I_2O_5 and HIO_3 crystals/droplets were studied using an optical microscope (Olympus BX51) coupled to a home-made temperature and humidity controlled stage (Murray et al., 2010a, b). A schematic diagram of this equipment is shown in Fig. 1.

The water vapour pressure in the N_2 gas flow through the chamber was controlled by passing the gas through a liquid water bubbler and a trap which were immersed in a coolant mixture (50:50 ethylene glycol and water) in a temperature controlled bath (Haake K40). The bubbler served to humidify the flow and the trap (a glass bubbler with only condensation on its walls) served to remove extra water vapour resulting from aerosol formation associated with bubble bursting in the bubbler. The water vapour pressure passing into the cell could therefore be controlled by changing the temperature of the bath between 0 °C and room temperature and for lower dew points the flow was diluted with dry N_2. The humidified and dry flows were quantified using mass flow

controllers (MKS 1179). The temperature of the bubbler and trap were recorded using a calibrated thermocouple.

The temperature of the stage was set using a temperature controller (Eurotherm 2416) and heaters (2×35 W) embedded in the cold stage which was cooled with a constant flow of cold gas from a pressurised liquid nitrogen dewar. The relative humidity around the droplet/particles in the chamber is the ratio of the partial pressure of water in the gas phase, defined by the bubbler temperature, to the equilibrium vapour pressure of water at the temperature of the stage. The temperature dependent parameterisation for the equilibrium vapour pressure of water was taken from the literature (Murphy and Koop, 2005).

Deliquescence: crystals of I_2O_5 and HIO_3 (typical sizes of 10–50 µm) were placed onto a hydrophobic glass slide which had been pre-cleaned in Piranha solution (H_2SO_4:H_2O_2 mixture), rinsed with 18.2 MΩ water and methanol, and then silanised using a 5% solution of dichloro-dimethylsilane in heptane. Aqueous droplets supported on surfaces prepared in this manner have a contact angle of ~100° and do not induce phase changes (Murray et al., 2010a, b; Dymarska et al., 2006; Eastwood et al., 2009). The slide was then placed on the cold stage of the instrument under the optical microscope which was connected to a grey-scale digital camera (Hitachi). Images were viewed on a monitor and recorded digitally using a commercial DVD recorder. Relative humidity and temperature data were logged during the course of an experiment.

Efflorescence: aqueous droplets formed in the deliquescence experiments were subsequently exposed to decreasing RH down to ~0% RH while monitoring the microscope images for evidence of crystallisation.

The deliquescence/efflorescence set-up was initially tested using ammonium sulphate crystals (>99.0%, Aldrich), and gave very good agreement (to within ± 1%, our uncertainty in RH) with values reported in a number of laboratory studies e.g. a DRH of 80 ± 1% and ERH of 32 ± 1% at 298 K (Tang and Munkelwitz, 1993; Onasch et al., 1999) and those calculated using the AIM aerosol thermodynamics model (e.g. Clegg et al., 1998).

3 Results and discussion

3.1 Water activity measurements

The measured water activity (a_w) at 293 K for solutions with a range of iodate concentrations made up with I_2O_5 and HIO_3 are plotted in Fig. 2.

The data points shown at highest molality correspond to the water activities of iodate solutions for saturated solutions of I_2O_5 (we used our measurement of solubility derived later in this paper rather than the value given in the CRC handbook, Lide, 2009). The plotted data was fitted using a fifth order polynomial function for which the coefficient values and functional form are shown in Table 1.

It can be seen from Fig. 2 that the water activity decreases steadily with increasing molality as expected. However, the data shows a positive deviation from ideality [assuming full dissociation of both compounds into the respective ions in solution and that $a_w = v_{H_2O} / (v_{H_2O} + v_{ions})$, where v is the number of moles (Sereno et al., 2001; Caurie, 1983)] at all m values up to I_2O_5 saturation where a_w (ideal)=0.60 compared with the measured value of 0.80 ± 0.01. This positive deviation is consistent with the complex solution structures previously reported from conductance measurements (Pethybridge and Prue, 1967), which identified the ionic species, $H(IO_3)_2^-$ (from association of $HIO_3 + IO_3^-$) in dilute solutions, and by Goldman et al. (1974) who identified an increasing degree of molecular association (HIO_3 dimers, trimers and tetramers) at higher concentrations.

3.2 Density measurements

The measured density data at 293 K is shown in Fig. 3 for a number of HIO_3 and I_2O_5 solutions up to saturation, as a function of $m(IO_3^-)$. A fifth order polynomial function was used to fit the density data – see Table 1 for the function and coefficients.

3.3 Viscosity measurements

Measured viscosity data for $15.8 \leq m(\mathrm{IO}_3^-) \leq 17.6 \, \mathrm{moles\,kg}^{-1}$ at 303 K for aqueous solutions are plotted in Fig. 4 as a function of $m(\mathrm{IO}_3^-)$, along with the data reported by Nayar et al. (1939) for $m \leq 4 \, \mathrm{moles\,kg}^{-1}$. Figure 4 shows a rapidly increasing solution viscosity at higher concentrations (with $\eta = 97 \pm 1$ cP at saturation i.e. ~2 orders of magnitude greater than η_{water} at 303 K i.e. ~0.8 cP, Korson et al., 1969), for which a best fit exponential function is given in the figure caption.

At lower temperature, for an equivalent solution molality, higher viscosities were observed. The data measured at 293, 298 and 303 K for solutions of $15.8 \leq m(\mathrm{IO}_3^-) \leq 17.6 \, \mathrm{moles\,kg}^{-1}$ are shown in an Arrhenius plot in Fig. 5.

From this figure, the viscosity trends of these concentrated solutions are consistent with first order fluid behaviour i.e. exponentially decreasing viscosity with increasing temperature for all m (see Table 2 for fitted parameters).

While the temperature dependence of viscosity of these solutions approximates well to an Arrhenius law, it is well known that the Arrhenius law under-predicts the temperature dependence of many aqueous solutions (Angell, 2002; Murray, 2008b). Hence, extrapolation of the fit to lower temperatures only provides a lower limit to viscosity. Bearing this in mind, for a saturated solution the fit yields a viscosity of 5054 cP at 253 K – a temperature relevant for marine polar regions. This suggests iodate solution droplets become very viscous under atmospherically relevant conditions and this may have important implications for their growth through uptake of other condensable vapours. More concentrated solutions would be even more viscous. Implications of this are discussed in more detail later.

20831

3.4 Deliquescence and efflorescence behaviour

3.4.1 Deliquescence

Figure 6 shows a sequence of recorded images from an $\mathrm{I}_2\mathrm{O}_5$ deliquescence experiment at $T = 298$ K. The RH was increased across the deliquescence point in increments of 0.5% and the droplets left for 5 minutes at each increment.

Panel (i) shows solid crystals on the sample slide under dry N_2 gas; (ii) shows that at RH = $78.8 \pm 1.0\%$, which is just below the deliquescence RH, the crystals are unchanged; (iii) shows crystals beginning to take up water at RH = $79.5 \pm 1.0\%$, whilst panel (iv) shows fully deliquesced aqueous droplets at RH = $80.0 \pm 1.0\%$. From these images we determine the DRH of $\mathrm{I}_2\mathrm{O}_5$ at 298 K as $79.5 \pm 1.0\%$. These experiments were repeated for a range of temperatures for both HIO_3 and $\mathrm{I}_2\mathrm{O}_5$ (from 273–303 K). The results are given in Table 3.

The DRH values of HIO_3 (85.0 ± 1.0 %) and $\mathrm{I}_2\mathrm{O}_5$ ($80.8 \pm 1.0\%$) at 293 K are in good agreement with the measured water activity (%DRH = a_w of a saturated solution × 100, when the aqueous droplet is in equilibrium with water vapour) for saturated solutions ($a_w = 0.84 \pm 0.01$ for HIO_3 and $a_w = 0.80 \pm 0.01$ for $\mathrm{I}_2\mathrm{O}_5$) at this temperature (see Fig. 2).

Differences in the crystalline structures and chemical potential of HIO_3 and $\mathrm{I}_2\mathrm{O}_5$ (Rogers, 1941; Selte and Kjekshus, 1970) are reflected in the differing DRH values for each compound. Although these two solids form identical aqueous solutions, they will have different enthalpies of solution ($\Delta \mathrm{H}_{\mathrm{sol}}$). This parameter can be derived from temperature-dependent DRH measurements following the method outlined by Tang and Munkelwitz (1993), if temperature-dependent solubility data is available for the solid in question. Such data does not exist in the literature for $\mathrm{I}_2\mathrm{O}_5$, but is known for HIO_3 over the range 273–373 K (Lide, 2009).

The enthalpy of solution can be evaluated by applying the Clausius-Clapeyron equation for the phase transformation, as given by,

$$\frac{d \ln a_w}{dT} = -\frac{n \Delta \mathrm{H}_{\mathrm{sol}}}{RT^2} \qquad (3)$$

20832

where R is the gas constant, and a_w is defined as:

$$a_w = \frac{p}{p^o} = \frac{\%DRH}{100} \tag{4}$$

Where p refers to the saturation vapour pressure of water, and p^o refers to the equilibrium vapour pressure of pure water at temperature T. The solubility (n) in moles of solute per moles of water can be expressed as a quadratic function of T:

$$n = A + BT + CT^2 \tag{5}$$

The values of the coefficients A, B, and C can therefore be calculated from a fit of solubility data at different temperatures. For HIO_3 the fitted coefficient values are as follows: $A = 1.998$, $B = -1.310 \times 10^{-2}$, $C = 2.500 \times 10^{-5}$.

We derived temperature dependent solubility values for I_2O_5 using our measurements of water activity and temperature dependent deliquescence RH values. The deliquescence point is the RH at which a crystal is in equilibrium with a saturated solution. Since the water activity of a saturated solution is equal to the RH, the DRH is equal to the water activity of a saturated solution. We therefore used our measured relationship between water activity and molality to determine the molality of a saturated solution. In order to do this we assume that water activity is independent of temperature, which is a good approximation for many aqueous solutions (Koop, 2004; Kitic et al., 1986). The calculated aqueous solubility at a number of temperatures for I_2O_5 is given in Table 4.

Fitting Eq. (5) to this data yields the following solubility coefficients: $A = 6.124 \times 10^{-1}$, $B = -3.751 \times 10^{-3}$, $C = 7.289 \times 10^{-6}$. The CRC handbook gives a value of 253.4 g/100 g water at 293 K, whereas we find a value of 258.0 ± 3.5 g/100 g water at the same temperature.

For verification of this method of determining solubility, the solubility of HIO_3 at various temperatures was calculated using the measured DRH and a_w values. The calculated values of solubility were found to be in good agreement with the data given in the CRC Handbook (Lide, 2009).

For calculation of the enthalpy of solution (ΔH_{sol}), the expressions for n from Eq. (5) and DRH from Eq. (4) were substituted into Eq. (3), and on integrating the resulting equation with respect to T, we find;

$$\ln DRH = \frac{\Delta H_{sol}}{R} \left[\frac{A}{T} - B\ln T - CT \right] + I \tag{6}$$

where I is the integration constant.

Equation (6) therefore predicts a linear fit when values of ln(DRH) are plotted against the function ($A/T - B\ln T - CT$) with a slope of $\Delta H_{sol}/R$. Figures 7 and 8 show such plots for the HIO_3 and I_2O_5 data respectively. The calculated value of ΔH_{sol} from the fitted data in Fig. 7 of 8.3 ± 0.7 kJ mol^{-1} is consistent with the value quoted in the CRC Handbook of $+8.8$ kJ mol^{-1}. For I_2O_5, the calculated value of ΔH_{sol} from the slope of the fit shown in Fig. 8 is 12.4 ± 0.6 kJ mol^{-1}. This represents the first determination of this quantity that we are aware of.

As a test for the procedure described above, the measured DRH variation for ammonium sulphate (Sect. 2.4) was used along with solubility data from the literature (Tang and Munkelwitz, 1993) to fit the enthalpy of solution for this compound. The calculated value for ΔH_{sol} of 5.9 ± 0.5 kJ mol^{-1} is in good agreement with the literature value of $+6.3$ kJ mol^{-1}.

Finally, the solubility coefficients A, B and C and evaluated ΔH_{sol} were implemented in the defining equation linking the theoretical DRH (%) variation with temperature (Tang and Munkelwitz, 1993);

$$DRH(T) = DRH(T_o) \exp \left[\frac{\Delta H_{sol}}{R} \left\{ A \left(\frac{1}{T} - \frac{1}{T_o} \right) - B\ln \left(\frac{T}{T_o} \right) - C(T - T_o) \right\} \right] \tag{7}$$

Where T_o is a reference temperature and DRH (T_o) is the reference value of DRH at this temperature. In our experiments, T_o is taken at 293 K and the measured water activity of a saturated solution of HIO_3 and I_2O_5 at this temperature was used to evaluate DRH (T_o). Measured deliquescence data for $(NH_4)_2SO_4$, HIO_3, and I_2O_5 crystals at

273 < T < 303 K and the corresponding theoretical lines based on Eq. (7) are shown in Fig. 9.

The DRH values determined using Eq. (7) for HIO_3 and I_2O_5 were extrapolated to 250 K in Fig. 10 in order to estimate values applicable to a variety of marine locations (temperate to polar).

From this figure, the expected DRH values of HIO_3 and I_2O_5 at 253 K are determined at 97.2 ± 1.0% and 88.5 ± 1.0% respectively. However, under these conditions the atmosphere is supersaturated with respect to ice. If IOPs are initially crystalline, they may either deliquesce at high humidity or possibly serve as ice nuclei above ice saturation and below deliquescence.

3.4.2 Efflorescence behaviour

Freshly deliquesced droplets of both HIO_3 and I_2O_5 on glass slides were subsequently exposed to decreasing RH values down to "dry" conditions (<1% RH). Initially, RH was ramped down at intervals of 2% down to 60% and the droplets were left to equilibrate at each RH interval for 10 min. Then the RH was reduced in intervals of 10% to about 10%, but leaving the droplets for 1 hour at each interval. After this droplets were left for 2 h at <1% RH and then on the following day the same droplets were left at <1% RH for 7 h. During these experiments, crystallisation was not observed.

Figure 11 shows a sequence of images for efflorescence experiments with $(NH_4)_2SO_4$, and iodate solutions made up with both HIO_3 and I_2O_5. Efflorescence of the $(NH_4)_2SO_{4(aq)}$ droplets is clearly evident at RH ~32% whilst droplets of both HIO_3 and I_2O_5 show no such behaviour down to the lowest RH levels which indicates that they remained non-crystalline.

This result is intriguing given that sub-saturated iodate solutions become increasingly viscous at higher concentrations. This trend is likely to continue as the iodate solutions become supersaturated as the RH is lowered below DRH. It is known that many aqueous solutions can become glassy at high concentration (Zobrist et al., 2008; Murray, 2008a; Murray and Bertram, 2008; Mikhailov et al., 2009; Murray et al., 2010c). Further

work is required to see if iodate solutions become glassy under atmospherically relevant conditions.

4 Conclusions and atmospheric implications

We report the first quantitative measurements of the molality-dependent water activity, solution density and viscosity for aqueous iodate solutions as well as the first measurements of the deliquescence humidity of crystalline I_2O_5 and HIO_3. As discussed in the introduction, these compounds are likely to result from iodine-containing vapours released into the marine atmosphere. This physical data is crucial for evaluating the role of iodine oxide particles (IOPs) in the marine atmosphere.

In terms of the reported deliquescence properties, it should be noted that a number of studies of the hygroscopic behaviour of nanoparticles (<20 nm diameter) of inorganic salts indicate a distinct "size effect" with an increase in characteristic DRH level (above that for larger solid particles or bulk, crystalline samples) due to surface tension/forces resulting at such small particle sizes (Hameri et al., 2000, 2001; Russell and Ming, 2002; Biskos et al., 2006). The temperature-dependent values reported in our study therefore are likely to represent lower limits for deliquescence of crystalline IOPs in the marine atmosphere. Indeed, a recent laboratory study of the hygroscopic behaviour of freshly nucleated IOPs (<10 nm in diameter) reported no observable particle growth or evidence of deliquescence up to RH=90% (Saunders et al., 2010). However, if local iodine source and particle growth rates are high enough e.g. at seaweed-rich coastal areas, it has been shown (Mahajan et al., 2010) that IOPs can grow rapidly enough to overcome scavenging by background (sea-salt) aerosol and grow to sizes (>50 nm) where deliquescence could take place at 80%<RH<90%.

Our studies of iodate solution droplets at low humidity indicate that they do not effloresce even when left at below 1% RH for many hours. This observation suggests that deliquesced IOPs (formed in humid environments) will remain in a non-crystalline metastable aqueous state. This may have implications for the uptake of other volatile

chemical species and the subsequent growth rates of IOPs. Our viscosity measurements indicate that these iodate solution droplets become increasingly viscous at lower temperatures and higher concentrations, which raises the possibility that they may become glassy under atmospherically relevant conditions. Future studies should focus on the properties of metastable supersaturated iodate solutions and their apparent inability to crystallise.

References

Angell, C. A.: Liquid fragility and the glass transition in water and aqueous solutions, Chem. Rev., 102, 2627–2650, 2002.

Biskos, G., Paulsen, D., Russell, L. M., Buseck, P. R., and Martin, S. T.: Prompt deliquescence and efflorescence of aerosol nanoparticles, Atmos. Chem. Phys., 6, 4633–4642, doi:10.5194/acp-6-4633-2006, 2006.

Burkholder, J. B., Curtius, J., Ravishankara, A. R., and Lovejoy, E. R.: Laboratory studies of the homogeneous nucleation of iodine oxides, Atmos. Chem. Phys., 4, 19–34, doi:10.5194/acp-4-19-2004, 2004.

Caurie, M.: Raoult's law, water activity and moisture availability in solutions, J. Food Sci., 48, 648–649, 1983.

Clegg, S. L., Brimblecombe, P., and Wexler, A. S.: Thermodynamic model of the system H^+-NH_4^+-SO_4^{2-}-NO_3^--H_2O at tropospheric temperatures, J. Phys. Chem. A, 102, 2137–2154, 1998.

Daehlie, G. and Kjekshus, A.: Iodine oxides: Part I. On $I_2O_3.SO_3$, $I_2O_3.4SO_3.H_2O$, $I_2O_3.SeO_3$ and I_2O_4, Acta Chem. Scand., 18, 144–156, 1964.

Dymarska, M., Murray, B. J., Sun, L. M., Eastwood, M. L., Knopf, D. A., and Bertram, A. K.: Deposition ice nucleation on soot at temperatures relevant for the lower troposphere, J. Geophys. Res., 111, D04204, doi:10.1029/2005JD006627, 2006.

Eastwood, M. L., Cremel, S., Wheeler, M., Murray, B. J., Girard, E., and Bertram, A. K.: The effects of sulfuric acid and ammonium sulfate coatings on the ice nucleation properties of kaolinite particles, Geophys. Res. Lett., 36, L02811 doi:02810.01029/02008GL035997, 2009.

Gilfedder, B. S., Lai, S. C., Petri, M., Biester, H., and Hoffmann, T.: Iodine speciation in rain, snow and aerosols, Atmos. Chem. Phys., 8, 6069–6084, doi:10.5194/acp-8-6069-2008, 2008.

Goldman, S., Bates, R. G., and Robinson, R. A.: Osmotic coefficients and activity coefficients of iodic acid at high concentrations, J. Sol. Chem., 3, 593–602, 1974.

Groschuff, E.: On iodic acid, Z. Anorg. Chem., 47, 331–352, 1905.

Hameri, K., Vakeva, M., Hansson, H. C., and Laaksonen, A.: Hygroscopic growth of ultrafine ammonium sulphate aerosol measured using an ultrafine tandem differential mobility analyzer, J. Geophys. Res., 105, 22231–22242, 2000.

Hameri, K., Laaksonen, A., Vakeva, M., and Suni, T.: Hygroscopic growth of ultrafine sodium chloride particles, J. Geophys. Res., 106, 20749–20757, 2001.

Kitic, D., Jardim, D. C. P., Favetto, G. J., Resnik, S. L., and Chirife, J.: Theoretical prediction of water activity of standard saturated salt-solutions at various temperatures, J. Food Sci., 51, 1037–1041, 1986.

Koop, T.: Homogeneous ice nucleation in water and aqueous solutions, Z. Phys. Chem., 218, 1231–1258, 2004.

Korson, L., Drost-Hansen, W., and Millero, F. J.: Viscosity of water at various temperatures, J. Phys. Chem., 73, 34–39, 1969.

Lide, D. R.: CRC Handbook of Chemistry and Physics, 90th Ed., CRC, Boca Raton, 2009.

McFiggans, G., Coe, H., Burgess, R., Allan, J., Cubison, M., Alfarra, M. R., Saunders, R., Saiz-Lopez, A., Plane, J. M. C., Wevill, D., Carpenter, L., Rickard, A. R., and Monks, P. S.: Direct evidence for coastal iodine particles from Laminaria macroalgae – linkage to emissions of molecular iodine, Atmos. Chem. Phys., 4, 701–713, doi:10.5194/acp-4-701-2004, 2004.

McFiggans, G., Artaxo, P., Baltensperger, U., Coe, H., Facchini, M. C., Feingold, G., Fuzzi, S., Gysel, M., Laaksonen, A., Lohmann, U., Mentel, T. F., Murphy, D. M., O'Dowd, C. D., Snider, J. R., and Weingartner, E.: The effect of physical and chemical aerosol properties on warm cloud droplet activation, Atmos. Chem. Phys., 6, 2593–2649, doi:10.5194/acp-6-2593-2006,

2006.

McFiggans, G., Bale, C. S. E., Ball, S. M., Beames, J. M., Bloss, W. J., Carpenter, L. J., Dorsey, J., Dunk, R., Flynn, M. J., Furneaux, K. L., Gallagher, M. W., Heard, D. E., Hollingsworth, A. M., Hornsby, K., Ingham, T., Jones, C. E., Jones, R. L., Kramer, L. J., Langridge, J. M., Leblanc, C., LeCrane, J.-P., Lee, J. D., Leigh, R. J., Longley, I., Mahajan, A. S., Monks, P. S., Oetjen, H., Orr-Ewing, A. J., Plane, J. M. C., Potin, P., Shillings, A. J. L., Thomas, F., von Glasow, R., Wada, R., Whalley, L. K., and Whitehead, J. D.: Iodine-mediated coastal particle formation: an overview of the Reactive Halogens in the Marine Boundary Layer (RHaMBLe) Roscoff coastal study, Atmos. Chem. Phys., 10, 2975–2999, doi:10.5194/acp-10-2975-2010, 2010.

Mahajan, A. S., Plane, J. M. C., Oetjen, H., Mendes, L., Saunders, R. W., Saiz-Lopez, A., Jones, C. E., Carpenter, L. J., and McFiggans, G. B.: Measurement and modelling of tropospheric reactive halogen species over the tropical Atlantic Ocean, Atmos. Chem. Phys., 10, 4611–4624, doi:10.5194/acp-10-4611-2010, 2010.

Martin, S.: Phase transitions of aqueous atmospheric particles, Chem. Rev., 100, 3403–3453, 2000.

Mikhailov, E., Vlasenko, S., Martin, S. T., Koop, T., and Pöschl, U.: Amorphous and crystalline aerosol particles interacting with water vapor: conceptual framework and experimental evidence for restructuring, phase transitions and kinetic limitations, Atmos. Chem. Phys., 9, 9491–9522, doi:10.5194/acp-9-9491-2009, 2009. Bibtex EndNote Reference Manager XML

Murphy, D. M. and Koop, T.: Review of the vapour pressures of ice and supercooled water for atmospheric applications, Q. J. Roy. Meteorol. Soc., 131, 1539–1565, 2005.

Murray, B. J.: Inhibition of ice crystallisation in highly viscous aqueous organic acid droplets, Atmos. Chem. Phys., 8, 5423–5433, doi:10.5194/acp-8-5423-2008, 2008a.

Murray, B. J.: Enhanced formation of cubic ice in aqueous organic acid droplets, Env. Res. Lett., 3, 025008, doi:10.1088/1748-9326/3/2/025008, 2008b.

Murray, B. J. and Bertram, A. K.: Inhibition of solute crystallisation in aqueous H^+- NH_4^+-SO_4^{2-}-H_2O droplets, Phys. Chem. Chem. Phys., 10, 3287–3301, 2008.

Murray, B. J., Broadley, S. L., Wilson, T. W., Bull, S., Wills, R. H., Christenson, H. K., and Murray, E. J.: Kinetics of the homogeneous freezing of water, Phys. Chem. Chem. Phys., 12, 10380–10387, doi:10.1039/c003297b, 2010a.

Murray, B. J., Wilson, T. W., Broadley, S. L., and Wills, R. H.: Heterogeneous freezing of water droplets containing kaolinite and montmorillonite particles, Atmos. Chem. Phys. Discuss.,

20839

10, 9695–9729, doi:10.5194/acpd-10-9695-2010, 2010b.

Murray, B. J., Wilson, T. W., Dobbie, S., Cui, Z. Q., Al-Jumur, S., Mohler, O., Schnaiter, M., Wagner, R., Benz, S., Niemand, M., Saathoff, H., Ebert, V., Wagner, S., and Karcher, B.: Heterogeneous nucleation of ice particles on glassy aerosols under cirrus conditions, Nature Geosci., 3, 233–237, 2010c.

Nayar, M. R., Srivastava, L. N., Sen, A. B., Gopal, R., and Sharma, P. N.: The constitution of iodic acid. III, Z. Anorg. Allg. Chem., 240, 217–231, 1939.

O'Dowd, C. D., Hämeri, K., Mäkelä, J. M., et al.: A dedicated study of new particle formation and fate in the coastal environment (PARFORCE): Overview of objectives and achievements, J. Geophys. Res., 107, 8108, doi:10.1029/2001JD000555, 2002a.

O'Dowd, C. D., Jimenez, J. L., Bahreini, R., et al.: Marine aerosol formation from biogenic iodine emissions, Nature, 417, 632–636, 2002b.

O'Dowd, C. D. and De Leeuw, G.: Marine aerosol production: A review of the current knowledge, Philos. T. Roy. Soc. London A, 365, 1753–1774, 2007.

Onasch, T. B., Siefert, R. L., Brooks, S. D., Prenni, A. J., Murray, B., Wilson, M. A., and Tolbert, M. A.: Infrared spectroscopic study of the deliquescence and efflorescence of ammonium sulfate aerosol as a function of temperature, J. Geophys. Res., 104, 21317–21326, 1999.

Pechtl, S., Schmitz, G., and von Glasow, R.: Modelling iodide iodate speciation in atmospheric aerosol: Contributions of inorganic and organic iodine chemistry, Atmos. Chem. Phys., 7, 1381–1393, doi:10.5194/acp-7-1381-2007, 2007.

Pethybridge, A. D. and Prue, J. E.: Equilibria in aqueous solutions of iodic acid, Trans. Faraday Soc., 63, 2019–2033, 1967.

Rogers, M. T. and Helmholz, L.: The crystal structure of iodic acid, J. Am. Chem. Soc., 63, 278–284, 1941.

Russell, L. M. and Ming, Y.: Deliquescence of small particles, J. Chem. Phys., 116, 311–321, 2002.

Saiz-Lopez, A., Mahajan, A. S., Salmon, R. A., Bauguitte, S. J. B., Jones, A. E., Roscoe, H. K., and Plane, J. M. C.: Boundary layer halogens in coastal Antarctica, Science, 317, 348–351, 2007.

Saunders, R. W. and Plane, J. M. C.: Formation pathways and composition of iodine oxide ultra-fine particles, Environ. Chem., 2, 299–303, 2005.

Saunders, R. W., Kumar, R., Mahajan, A. S., Murray, B. J., and Plane, J. M. C.: Studies of the formation and growth of aerosol from molecular iodine precursor, Z. Phys. Chem., 224,

20840

1095–1117, doi:10.1524/zpch.2010.6143, 2010.

Segur, J. B. and Oberstar, H. E.: Viscosity of glycerol and its aqueous solutions, Ind. Eng. Chem., 43, 2117–2120, 1951.

Seinfeld, J. H. and Pandis, S. N.: Atmospheric Chemistry and Physics: From air pollution to climate change, 2nd Ed., Wiley & Sons, Hoboken, NJ, 2006.

Selte, K. and Kjekshus, A.: Iodine oxides: Part III. The crystal structure of I_2O_5, Acta Chem. Scand., 24, 1912–1924, 1970.

Sereno, A. M., Hubinger, M. D., Comesana, J. F., and Correa, A.: Prediction of water activity of osmotic solutions, J. Food Eng., 49, 103–114, 2001.

Stoloff, L.: Calibration of water activity measuring instruments and devices: Collaborative study, J. Assoc. Off. Anal. Chem., 61, 1166–1178, 1978.

Strong, L. E. and Pethybridge, A. D.: Aqueous iodic acid – conductance and thermodynamics, J. Sol. Chem., 16, 841–855, 1987.

Tang, I. N. and Munkelwitz, H. R.: Composition and temperature-dependence of the deliquescence properties of hygroscopic aerosols, Atmos. Environ., 27, 467–473, 1993.

Topping, D. O., McFiggans, G. B., and Coe, H.: A curved multi-component aerosol hygroscopicity model framework: Part 1 – Inorganic compounds, Atmos. Chem. Phys., 5, 1205–1222, doi:10.5194/acp-5-1205-2005, 2005.

Wexler, A. S. and Clegg, S. L.: Atmospheric aerosol models for systems including the ions H^+, NH_4^+, Na^+, SO_4^{2-}, NO_3^-, Cl^-, Br^-, and H_2O, J. Geophys. Res., 107, 4207, doi:10.1029/2001JD000451, 2002.

Zobrist, B., Marcolli, C., Pedernera, D. A., and Koop, T.: Do atmospheric aerosols form glasses?, Atmos. Chem. Phys., 8, 5221–5244, doi:10.5194/acp-8-5221-2008, 2008.

Table 1. Polynomial coefficients for fits (see equations at the foot of the table) to measured water activity (a_w) and solution density (ρ) data (see Figs. 2 and 3 respectively) for iodate solutions at 293 K. Concentrations are expressed as the molality of IO_3^- [$m(IO_3^-)$].

Coefficients of water activity, a_w [a]		Coefficients of density, ρ/g cm^{-3} [b]	
A_1	-1.21×10^{-3}	B_1	3.05×10^{-2}
A_2	5.73×10^{-4}	B_2	2.03×10^{-2}
A_3	-2.19×10^{-4}	B_3	-2.41×10^{-3}
A_4	2.07×10^{-5}	B_4	8.12×10^{-5}
A_5	-6.65×10^{-7}	B_5	1.35×10^{-8}

[a] $a_w = 1 + \Sigma_{i=1-5}\left(A_i \times m^i\right)$

[b] $\rho = 0.997 + \Sigma_{i=1-5}\left(B_i \times m^i\right)$

Table 2. Fitted Arrhenius parameters for the temperature dependent viscosity data (see Fig. 5).

$m(IO_3^-)$/moles kg^{-1}	Viscosity coefficient (A)/cP	Activation energy (E_a)/kJ mol^{-1}
17.6	$1.94\pm0.03\times10^{-7}$	50.4 ± 1.2
17.3	$4.57\pm0.06\times10^{-7}$	47.7 ± 2.3
16.8	$9.38\pm0.06\times10^{-7}$	45.1 ± 1.9
15.8	$1.07\pm0.08\times10^{-6}$	42.2 ± 2.9

Table 3. Measured values of deliquescence relative humidity (DRH) for I_2O_5 and HIO_3 crystals from 273–303 K.

Temperature/ K	DRH [%] – I_2O_5, ±1%	DRH [%] – HIO_3, ±1%
273	84.5	90.9
278	83.3	89.4
283	82.7	87.4
288	81.2	86.7
293	80.8	85.0
298	79.5	83.5
303	78.3	81.1

Table 4. Calculated aqueous solubility of I_2O_5 from 273–303 K. These values are derived from our water activity and deliquescence measurements (see text).

Temperature/K	Solubility of I_2O_5/g per 100 g of H_2O Accuracy ±3.5 g per 100 g of H_2O
273	244.1
278	246.6
283	249.7
288	253.5
293	258.0
298	263.2
303	269.0
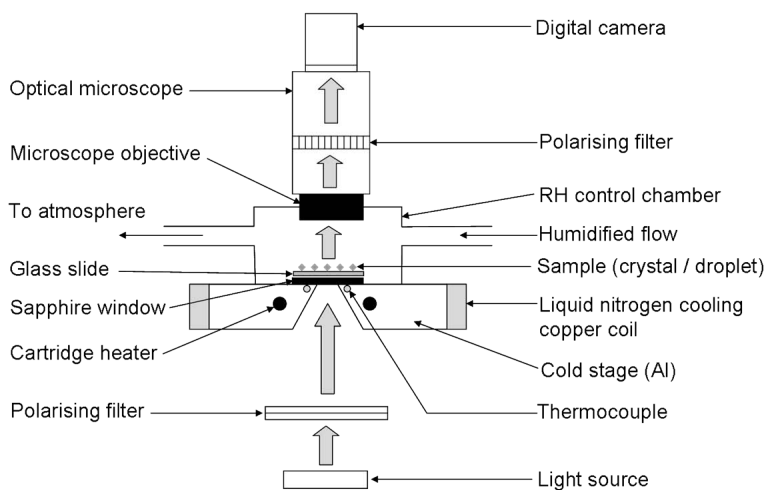
Fig. 1. Schematic depiction of the experimental set-up used to study the deliquescence of crystalline particles and the efflorescence of aqueous solution droplets.
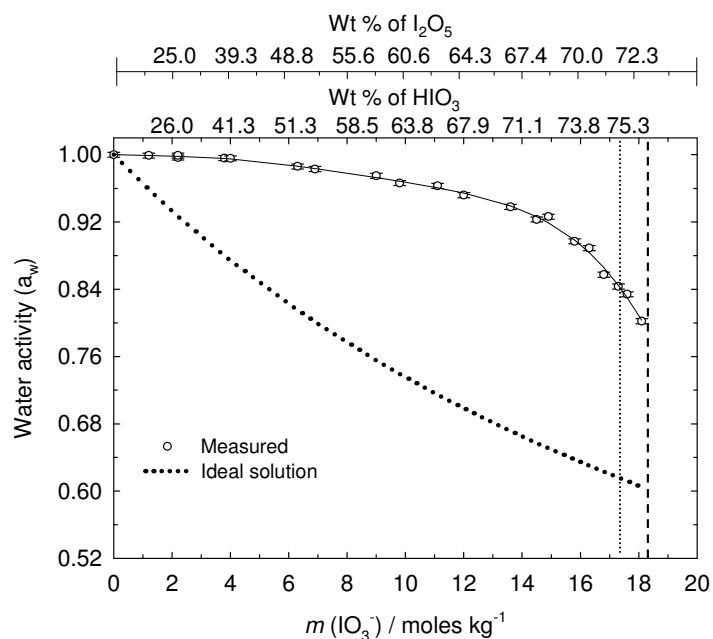
Fig. 2. Measured water activity values (open circles) at 293 K for aqueous solutions of IO_3^- from HIO_3/I_2O_5 over a range of molalities up to, and including that of a saturated solution of each solid. The solid line is a fifth order polynomial best-fit to the data (see Table 1). The vertical dashed line indicates the saturation molality for I_2O_5 and dotted line indicates the saturation molality for HIO_3 (or wt % – see top axis). The ideal water activity values (assuming full dissociation into ions) are indicated by the square dotted line.
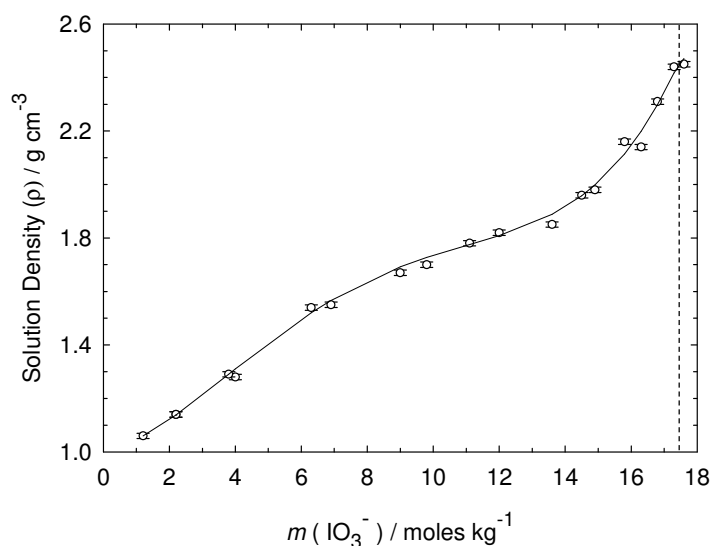
Fig. 3. Measured iodate solution densities at 293 K as a function of $m(IO_3^-)$ over a range of molalities up to and including that of a saturated solution of HIO_3. The solid line is a polynomial best-fit to the data (see Table 1). The vertical dashed line indicates the saturation molality of HIO_3.
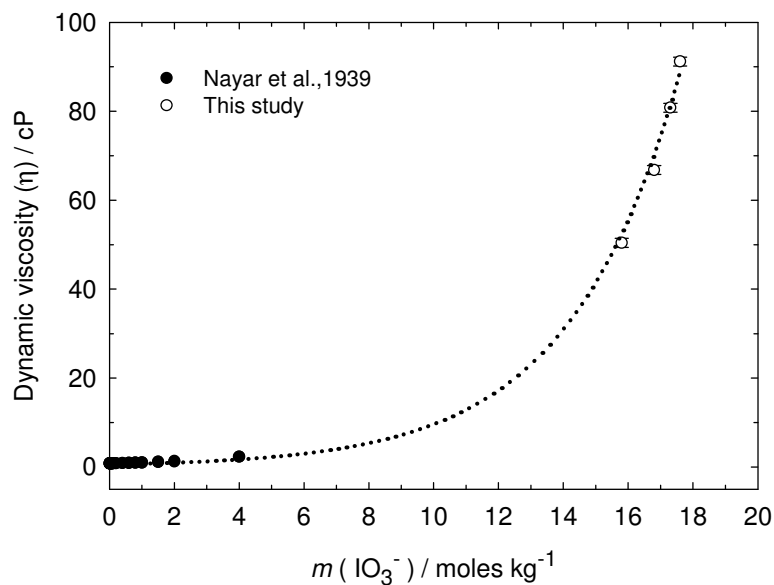
Fig. 4. Measured (open circles) and literature (filled circles) viscosity data for aqueous iodate solutions at 303 K, as a function of $m(IO_3^-)$. Our data is shown in addition to data from the literature (Nayar et al., 1939). The dotted line is a least-squares exponential fit ($\eta[cP] = 0.798\exp\{0.267 \times m\}$) through all data points.
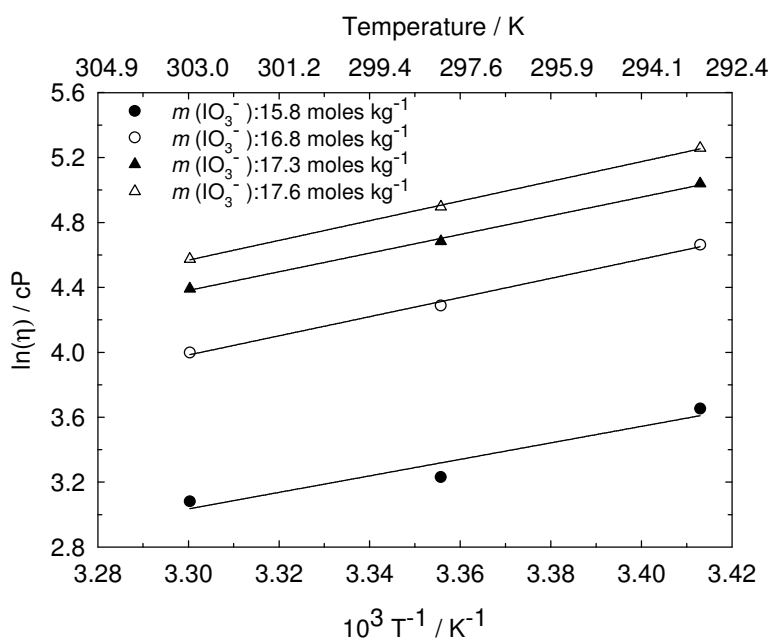
Fig. 5. Measured viscosity data for aqueous iodate solutions as a function of temperature, and associated linear fits (solid lines) using an Arrhenius equation of the form, $\ln(\eta)=\ln A+(E_a/RT)$ – see Table 2 for fitted values of A, (the pre-exponential viscosity coefficient), and E_a, (the activation energy).

(i) RH < 1%   (ii) RH = 78.8 ± 1.0%   (iii) RH = 79.5 ± 1.0%   (iv) RH =80.0 ±1.0%
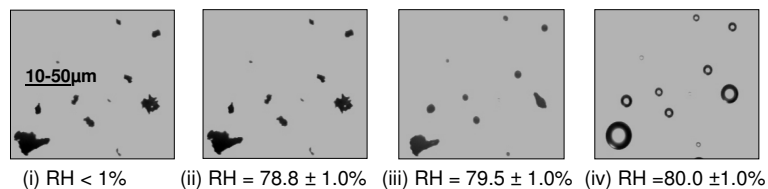
Fig. 6. A series of microscope images of I_2O_5 crystals at 298 K: (i) at low RH, (ii) just below the deliquescence point and (iii) at the point of deliquescence, and (iv) shows aqueous solution droplets.

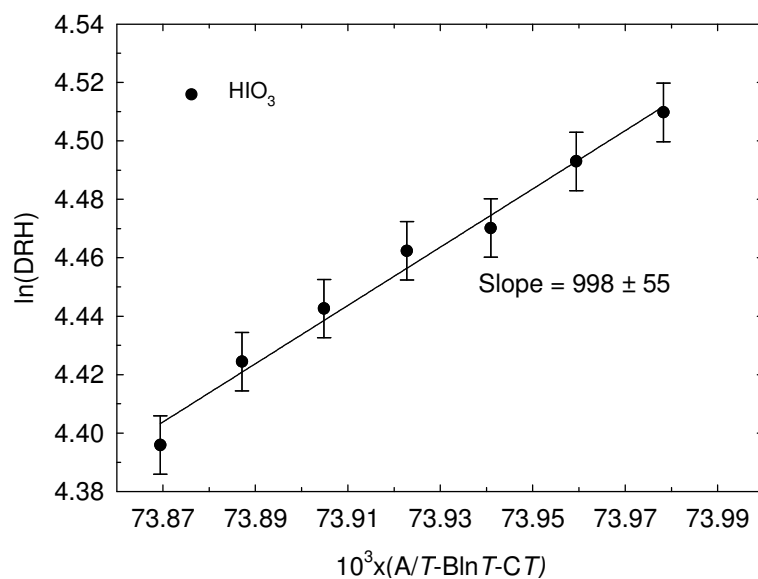**Fig. 7.** A plot of measured deliquescence RH values for HIO_3 against the temperature function which includes fitted solubility data (see Sect. 3.4).
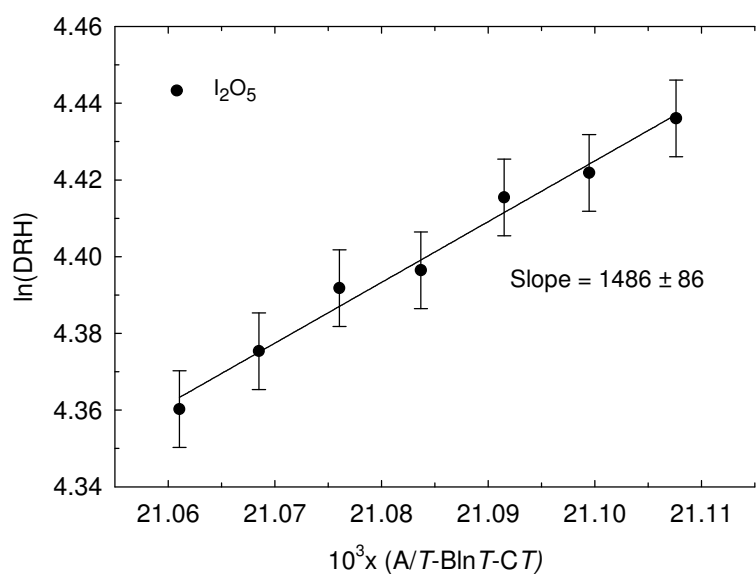
Fig. 8. A plot of measured deliquescence RH values for I_2O_5 against the temperature function which includes calculated solubility data (see Sect. 3.4).

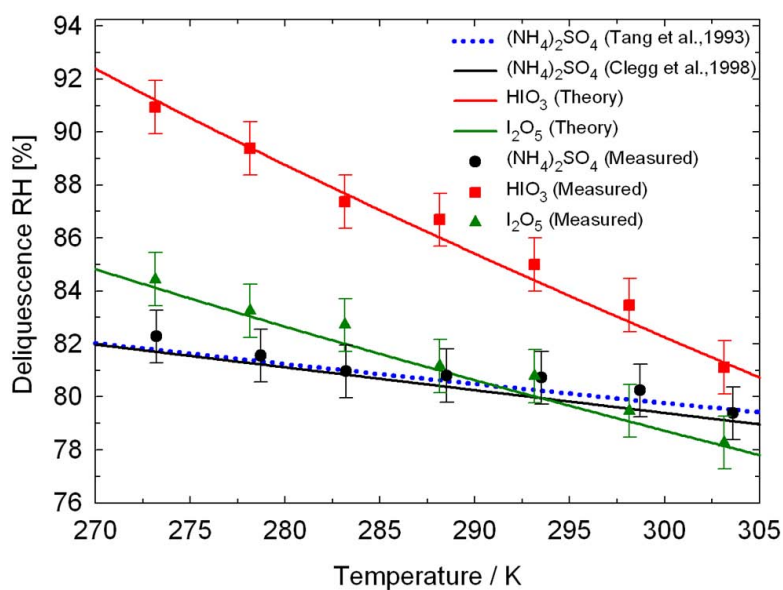**Fig. 9.** Measured DRH for $(NH_4)_2SO_4$, I_2O_5, and HIO_3 crystals as a function of temperature, and their corresponding theoretical fits calculated using Eq. (7) (see Sect. 3.4). Estimated errors in the measured data are ± 1% (RH).
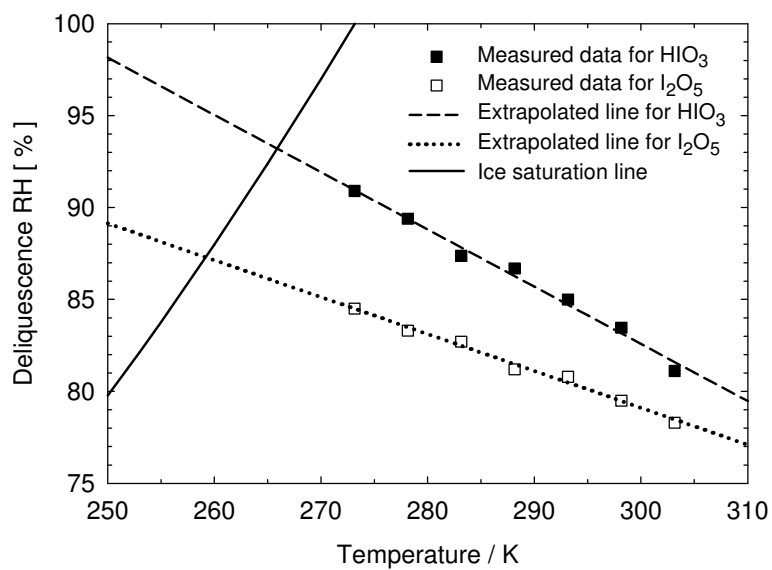
Fig. 10. Extrapolation of DRH fits of HIO_3 and I_2O_5 to lower temperatures. The solid line is the ice saturation line while dashed and dotted lines indicate the extrapolation of DRH data of HIO_3 and I_2O_5 respectively.
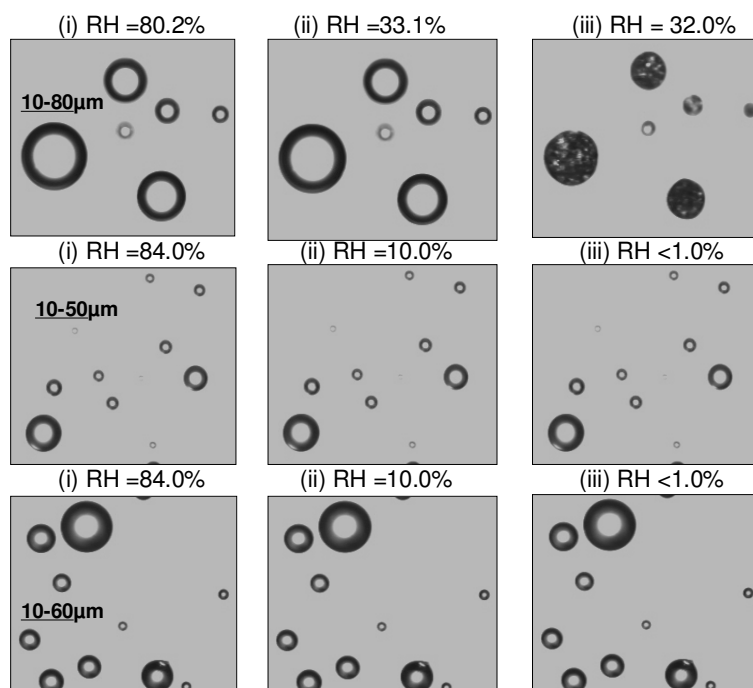
Fig. 11. A series of microscope images from the efflorescence experiments with droplets formed from crystals of $(NH_4)_2SO_4$ (top), I_2O_5 (middle), and HIO_3 (bottom).